Modeling the Stimulated Reservoir Volumes using DPDK Approach Coupled with Rock Mechanics*

Jack H. Deng[1], Zhangxing Chen[1], Jia Luo[1], Kun Wang[1], and Hui Liu[1]

Search and Discovery Article #42405 (2019)**
Posted August 5, 2019

*Adapted from oral presentation given at 2019 AAPG Annual Convention and Exhibition, San Antonio, Texas, May 19-22, 2019
 DOI:10.1306/42405Deng2019

[1]Schulich School of Engineering, University of Calgary, Calgary, Alberta, Canada (dengh@ucalgary.ca)

Abstract

A stimulation design involves a comprehensive engineering design procedure, which takes into account formation evaluation, fracturing fluid characterization, proppant transportation, rock mechanics, and ultimate stimulated reservoir volume (SRV) approximation through 3D fracture propagation modeling. The ultimate recovery is mainly controlled by fracture conductivity and SRV (Gidley et al., 1990), which are the key indicators to a stimulation success. Because of ultra-tight rock matrix permeability in a Nano-Darcy range for Tight Oil and Liquid Rich condensate reservoirs, propped fracture channels or a complex fracture network must maintain enough conductivity to achieve an economic production rate. Lab experiments using an API procedure showed that the fracture conductivity dropped several orders of magnitudes under the loading condition for various commercial fracturing proppants (Fredd et al. 2001). Therefore, modeling the fracture conductivity degradation vs. increasing net effective stress becomes a critical issue for a long-term production forecast. Modeling a hydraulically fractured unconventional tight sand reservoir is a coupled hydro-mechanical problem associated with complex interactions between dynamical fracture deformation under a loading condition and multiphase flow inside a fracture network. In this paper, a DPDK model with numerical MINC (multiple interacting continua) algorithms is utilized to represent the pressure transient within the tight matrix and interporosity flow from the matrix into a hybrid system consisting of a complex fracture network. The flow model is coupled with a FEM stress code to model the dynamical changing fracture aperture associated with increasing the effective normal stress during the pressure depletion. In addition, the choice of a coupling approach is critical because of the slow nonlinear convergence due to a significant increase in unknowns associated with poroelasticity equations. In this paper, the iterative coupling is adopted to solve the multiphase flow and stress equations using parallel computations because of its flexibility and efficiency compared to the fully coupled approach. A hydraulic fracture deformation mechanical model is developed and implemented into the PRSI framework. The fracture network closure is approximated by the Barton-Bandis hyperbolic deformation model, coupled with a modified Cubic Law based on a contact theory and validated by an API proppant test on proppant conductivity under loading stress. Finally, numerical examples on hydraulic fracture deformation will be presented. The coupled fluid flow-rock mechanics will illustrate the degradation of the fracture conductivity due to the increasing of normal stresses for a variety of proppant types.

References Cited

Bandis, S.C., A.C. Lumsden, and N.R. Barton, 1983, Fundamentals of Rock Joint Deformation: International Journal of Rock Mechanics and Mining Sciences & Geomechanics Abstracts December 31, v. 20/6, p. 249-268.

Barton, N.R., S.C. Bandis, and K. Bakhtar, 1985, Strength, Deformation and Conductivity Coupling of Rock Joints: International Journal of Rock Mechanics and Mining Sciences & Geomechanics Abstracts, v. 22/3, p. 121-140.

Chen, Z., 2005, Finite Element Methods and Their Applications. Scientific Computation: Springer, Berlin, Germany, ISBN-13 978-3-540-24078-5, 409 p.

Fredd, C.N., S.B. McConnell, C.L. Boney, and K.W. England, 2001, Experimental Study of Fracture Conductivity for Water-Fracturing and Conventional Fracturing Applications: SPE Journal, v. 6/3, p. 288-298. doi:10.2118/74138-PA

Gidley, J.L., S.A. Holditch, D.E. Nierode, and R.W. Veatch Jr., 1990, Recent Advances in Hydraulic Fracturing: SPE Monograph Series Vol. 12, ISBN: 978-1-55563-020-1, 464 p.

Kazemi, H., L.S. Merrill Jr., K.L. Porterfield, and P.R. Zeman, 1976, Numerical Simulation of Water-Oil Flow in Naturally Fractured Reservoirs: Society of Petroleum Engineers Journal, v. 16/6, p. 317-326.

Pruess, K., and T.N. Narasimhan, 1985, A Practical Method for Modeling Fluid and Heat Flow in Fractured Porous Media: Society of Petroleum Engineers Journal, v. 25/1, p. 14-26.

Whitson, C.H., and S. Sunjerga, 2012, PVT in Liquid-Rich Shale Reservoirs: SPE Annual Technical Conference and Exhibition, San Antonio, Texas, USA, 8-10 October, SPE-155499, 25 p. doi.org/10.2118/155499-MS

Modeling the Stimulated Reservoir Volumes using DPDK Approach Coupled with Rock Mechanics

J. H. Deng, Z. Chen, J. Luo, K. Wang, and H. Liu, University of Calgary

Outline

I. Research Objectives

II. Mathematical Model

I. Governing Equations (FVM) for Dual Porosity/Dual Permeability Model
II. MINC Formulation for nested submatrix volumes
III. Governing Equations (FEM) for Rock Mechanics
IV. Equivalent Continuum Constitutive Model

III. Coupled Rock Mechanics for Fracture Network Deformation

I. Coupled Fracture Deformation Model
II. Iterative Coupling Approach for Solving Flow-Stress Equations

IV. Numerical Experiments

I. Fracture deformation for natural joints
II. Dynamic 2nd fracture network deformation tuned by API proppant lab experiments

V. Conclusions

Modeling Approach

I. Numerical Representation of 2nd Fracture Network

I. A parallel control-volume multiphase multicomponent DPDK (dual porosity-dual permeability) model is implemented to solve the hybrid system consisting of 2nd fracture network and tight shale matrix

II. Numerical MINC (multiple interacting continua) algorithms is utilized to represent the transient pressure within the tight matrix and interporosity flow from the matrix into fracture network

II. Iteratively Coupled Dynamic Fracture Deformation Model

I. A FEM based rock mechanical model is established to build constitutive law, and to solve effective stress, strain and displacement unknowns using the equivalent continuum approach

II. Deformation of the fracture network is represented by Modified Barton-Bandis hyperbolic Model, and iteratively coupled with contact theory based cubic law.

AAPG ACE 2019 ANNUAL CONVENTION & EXHIBITION
19-22 May • San Antonio, Texas

SCHULICH School of Engineering

Research Objectives

I. During this research, for the multiphase flow within a hydraulically induced complex fracture network which resulted from massive slickwater stimulation, a **Dual Porosity/Dual Permeability model** with numerical MINC algorithms was adopted to predict the transient interporosity flow from tight matrix into the hybrid system which consists of hydraulic fracture planes and a complex 2nd fracture network.

II. In the numerical methods of modeling fractured rock mechanisms, the **equivalent continuum approach** is incorporated which transforms a complex and irregular fracture geometry system into regular spaced 3D fracture sets in the macroscopic level. An iterative flow-stress coupling algorithm is developed which allows the flexibility in data exchange between the flow and stress simulators.

III. Fracture closure is approximated by the **Barton-Bandis hyperbolic deformation model,** coupled with **contact theory based cubic law** and validated by API proppant tests under stress loading for various proppant strengths and concentrations.

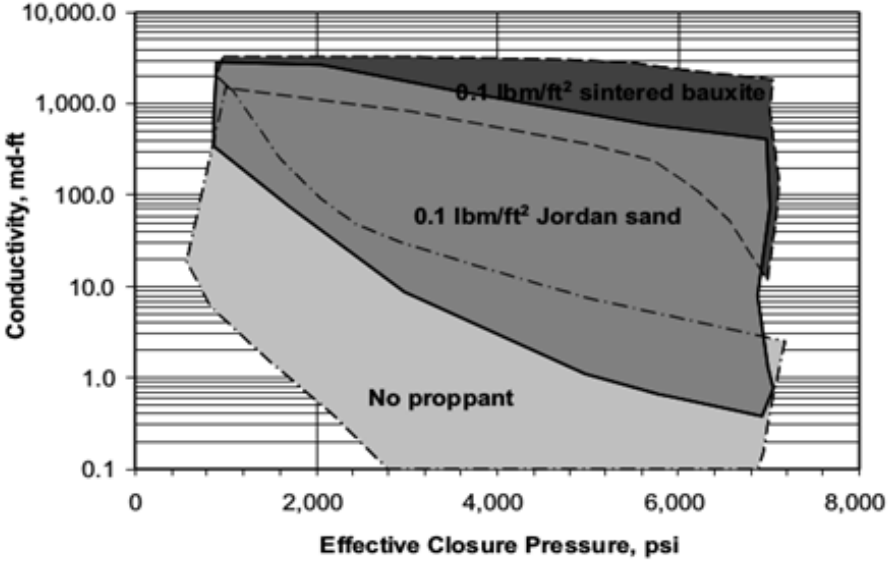

Proppant-filled fracture deformation under loading condition (Fred et al., 2001)

Governing Equations
DPDK Model

Mass Balance Equation:

$$\frac{\delta\left(\phi\sum_p \rho_p S_p x_{p,c}\right)}{\delta t} = \nabla\left(\sum_p \rho_p x_{p,c}\frac{Kk_{rp}}{\mu_p}\nabla\Phi_p\right) + \sum_p \rho_p x_{p,c}\dot{q}_p \quad c=[1,\ldots,N_c]$$

Accumulation Term *Flux Term* *Sink/Source Term*

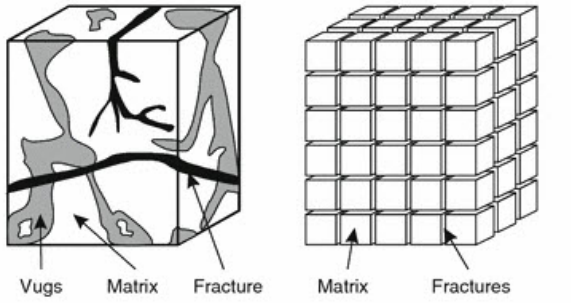

Mass Balance Equation for Matrix + Fracture:

$$Fracture: \nabla\left[\sum_i \left(\frac{K_f k_{f,r}}{\mu_f B_f}\right)_i \left(\nabla p_f - \rho_f g \nabla z\right)\right] = \frac{\delta\left(\phi_f \sum_i \frac{S_{fi}}{B_{fi}}\right)}{\delta t} + q_i + q_{mf}$$

Fracture Flow *Transfer Function*

$$Matrix: \nabla\left[\sum_i \left(\frac{K_m k_{m,r}}{\mu_m B_m}\right)_i \left(\nabla p_m - \rho_m g \nabla z\right)\right] = \frac{\delta\left(\phi_m \sum_i \frac{S_{mi}}{B_{mi}}\right)}{\delta t} - q_{mf}$$

Matrix to Matrix Flow

$$Matrix - Fracture - Transfer: \quad q_{mf} = \overline{kV}\left(\frac{k_{m,r}}{\mu_m B}\right)_i \sigma_{shape}\left(\Delta\Phi_m - \Delta\Phi_f\right)$$

Where

$$\sigma_{shape} = \frac{1}{4}\left(\frac{1}{l_x^2} + \frac{1}{l_y^2} + \frac{1}{l_z^2}\right)$$

Jacobian Matrix for Matrix and Fractures

Fracture Jacobian:

$$\overline{\overline{A}}_{ff} F + \overline{\overline{B}}_{fm} M = R_f$$

$$\left[\overline{\overline{A}}_{ff}\right]_m = \frac{\partial R^m_{accum}}{\partial X_f} + \frac{\partial R^m_{conv}}{\partial X_f} + \frac{\partial R^m_{source}}{\partial X_f} + \frac{\partial R^m_{m-f}}{\partial X_f}$$

$$\left[\overline{\overline{B}}_{fm}\right]_m = \frac{\partial R^m_{m-f}}{\partial X_m}$$

Matrix Jacobian:

$$\overline{\overline{C}}_{mf} F + \overline{\overline{D}}_{mm} M = R_m$$

$$\overline{\overline{C}}_{mf} = \frac{\partial R_m}{\partial X_f}$$

$$\overline{\overline{D}}_{mm} = \frac{\partial R_m}{\partial X_m}$$

The two residual equations yield a linear system:

$$\begin{pmatrix} \overline{\overline{A}}_{ff} & \overline{\overline{B}}_{fm} \\ \overline{\overline{C}}_{mf} & \overline{\overline{D}}_{mm} \end{pmatrix} \begin{pmatrix} F \\ M \end{pmatrix} = \begin{pmatrix} R_f \\ R_m \end{pmatrix}$$

F represents the fracture unknowns and **M** is for the matrix unknowns:

$F = \delta X_f$ and $M = \delta X_m$

MINC Formulation

The domain of investigation is discretized into nested computational volume elements format using the MINC approach (Pruess and Narasimhan, 1985).

Matrix System

$$Oil: \quad T^x_{om_{k-1/2}}\left(p^{n+1}_{om_{k-1}} - p^{n+1}_{om_k}\right) + T_{om_{k+1/2}}\left(p^{n+1}_{o_y} - p^{n+1}_{om_k}\right) - \frac{V_{b_k}}{\Delta t}\left[\left(\phi\frac{S_o}{B_o}\right)^{n+1}_{m_k} - \left(\phi\frac{S_o}{B_o}\right)^{n}_{m_k}\right] = 0$$

$$Water: T^x_{wm_{k-1/2}}\left(p^{n+1}_{wm_{k-1}} - p^{n+1}_{wm_k}\right) + T_{wm_{k+1/2}}\left(p^{n+1}_{w_y} - p^{n+1}_{wm_k}\right) - \frac{V_{b_k}}{\Delta t}\left[\left(\phi\frac{S_w}{B_w}\right)^{n+1}_{m_k} - \left(\phi\frac{S_w}{B_w}\right)^{n}_{m_k}\right] = 0$$

$$\begin{aligned} Gas: \quad & T^x_{om_{k-1/2}} R^x_{sm_{k-1/2}}\left(p^{n+1}_{om_{k-1}} - p^{n+1}_{om_k}\right) + T_{om_{k+1/2}} R^x_{sz}\left(p^{n+1}_{o_y} - p^{n+1}_{om_k}\right) \\ & + T^x_{gm_{k-1/2}} R^x_{sm_{k-1/2}}\left(p^{n+1}_{gm_{k-1}} - p^{n+1}_{gm_k}\right) + T_{gm_{k+1/2}} R^x_{sz}\left(p^{n+1}_{g_y} - p^{n+1}_{gm_k}\right) \\ & - \frac{V_{b_k}}{\Delta t}\left[\phi^{n+1}_{m_k}\left(\frac{R_s S_o}{B_o} + E_g S_g\right)^{n+1}_{m_k} - \phi^{n}_{m_k}\left(\frac{R_s S_o}{B_o} + E_g S_g\right)^{n+1}_{m_k}\right] = 0 \end{aligned}$$

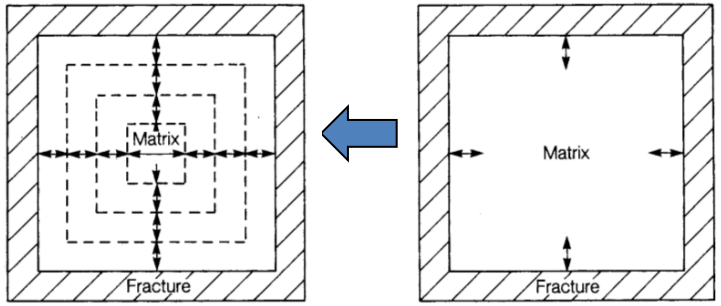

MINC matrix subdomains in nested meshes

The matrix is discretized into *M* levels of subdomains; the outer most matrix subdomain has the matrix-fracture transfer function

$$T_{mf_{k+1/2}}\left(p^{n+1}_{o_y} - p^{n+1}_{om_k}\right)$$

Between the *k-th* and *(k+1)-th* level, a matrix-matrix transfer term is applied between the cells

$$T^x_{om_{k-1/2}}\left(p^{n+1}_{om_{k-1}} - p^{n+1}_{om_k}\right)$$

Poroelastic Model for Fractured Rock

UNIVERSITY OF CALGARY

I. Stress Equilibrium Equation:

$$\nabla \cdot \sigma + \vec{f} = 0, \qquad X \in \Omega,$$

II. Effective Stress Equation:

$$\Delta\sigma_{ij}^{'} = \Delta\sigma_{ij} - \alpha_m \Delta p_m \delta_{ij} - \alpha_f \Delta p_f \delta_{ij}$$

$$\alpha_m = \frac{K_b\left(1 - \frac{K_*}{K_s}\right)}{K_*}, \alpha_f = 1 - \frac{K_b}{K_*}$$

III. Constitutive Law of Equivalent Continuum:

$$\Delta\varepsilon_{ij} = \Delta\varepsilon_{ij}^{m} + \Delta\varepsilon_{ij}^{f}$$

$$\begin{pmatrix} \Delta\mu_n \\ \Delta\mu_s \\ \Delta\mu_t \end{pmatrix} = \begin{pmatrix} \vec{n} & \vec{s} & \vec{t} \end{pmatrix} \begin{pmatrix} K_{nn} & 0 & 0 \\ 0 & K_{ss} & 0 \\ 0 & 0 & K_{tt} \end{pmatrix}^{-1} \begin{pmatrix} \vec{n} \\ \vec{s} \\ \vec{t} \end{pmatrix} \begin{pmatrix} \Delta\Gamma_n \\ \Delta\Gamma_s \\ \Delta\Gamma_t \end{pmatrix}$$

$$\Delta\varepsilon_{ij}^{f} = \sum_{nf}^{N_f} n_i^{nf} \Delta\mu_j^{nf} \frac{1}{S^{nf}}$$

$$\Delta\varepsilon_{ij}^{f} = C_{ijkl}^{f} \Delta\sigma_{kl}^{'}$$

$$C_{ijkl}^{f} = \sum_{nf}^{N_f} \frac{1}{S^{nf}} n_i^{nf} \sum_k c_{jk}^{nf} \sum_l n_l^{nf}$$

$$c_{jk} = \frac{1}{K_{nn}} n_j n_k + \frac{1}{K_{ss}} s_j s_k + \frac{1}{K_{tt}} t_j t_k$$

IV. Kinematics Equation:

$$\varepsilon_{ij} = \nabla u \equiv \frac{1}{2}(\nabla u + \nabla u^T) = \frac{1}{2}\left(\frac{\partial u_i}{\partial x_j} + \frac{\partial u_j}{\partial x_i}\right), \qquad i, j = 1, 2, 3.$$

V. Governing Equation:

$$\nabla \cdot \sigma + \vec{f} = 0, \qquad X \in \Omega,$$

$$\overline{\overline{\sigma}} = \overline{\overline{\sigma_0}} + \left(C_{ijkl}^{f} + C_{ijkl}^{m}\right)^{-1} \Delta\overline{\overline{\varepsilon}} + \left(\alpha_m \Delta p_m + \alpha_f \Delta p_f\right) \mathrm{I}$$

$$\Delta\overline{\overline{\varepsilon}} = \frac{1}{2}\left(\nabla \cdot \vec{u} + \left(\nabla \cdot \vec{u}\right)^T\right)$$

Governing Equation for Rock Mechanics

I. Governing Equation:

$$\int_{\Omega}\sigma_{ij}\left(\vec{u}\right)\varepsilon_{ij}\left(\vec{v}\right)d\Omega=\int_{\Omega}\vec{f}_{b}\cdot\vec{v}d\Omega+\int_{\partial\Omega 1}\vec{g^{s}}\cdot\vec{v}d\partial\Omega_{1}-\int_{\Omega}\sigma^{0}:\varepsilon\left(\vec{v}\right)d\Omega+\int_{\Omega}\alpha p\nabla\cdot\vec{v}d\Omega$$

Virtual internal energy

Virtual work done by the force acted on the object

II. Discretization and Partitioning (Chen, 2005):

Tetrahedron mesh partition of the concerned domain Ω

$$\Gamma_{h}=\left\{E_{i}:i=1,...,N\right\}$$

Finite Element Space:

$$\left(v_{h}^{k}\right)^{3}:=\left\{\vec{v}_{h}\in\left(C^{0}\left(\overline{\Omega}\right)\right)^{3}:\vec{v}_{h}\Big|_{E}\in\left(P\left(E\right)^{k}\right)^{3},\forall E\in\Gamma_{h}\right\}$$

$$\vec{u}_{h}\in\left(v_{h}^{k}\right)^{3}$$

$$a\left(\vec{u}_{h},\vec{v}_{h}\right)=L(\vec{v}_{h})\qquad\forall\vec{v}_{h}\in\left(v_{h}^{k}\right)^{3}$$

$$\int_{\Omega}B^{T}vDBu_{h}dx=\int_{\Omega}f\cdot vdx+\int_{\Gamma N}g\cdot vdl,\quad \mathrm{v}\in V_{h}$$

On each tetrahedron $K\in K_{h}$ the linear system can be written as

$$\int_{K}(B_{h}^{T}DB_{h})dxU=F+G$$

$$F=\left(\int_{K}f_{1}\lambda_{i}dx,\int_{K}f_{2}\lambda_{i}dx,\int_{K}f_{3}\lambda_{i}dx\right)_{i=1-4}^{T}$$

$$G=\left(\int_{\Gamma N}g_{1}\lambda_{i}dl,\int_{\Gamma N}g_{2}\lambda_{i}dl,\int_{\Gamma N}g_{3}\lambda_{i}dl\right)_{i=1-4}^{T}$$

Iterative Coupled Fluid Flow-Rock Mechanics Model

By implementing the ***true porosity*** and ***volumetric strain***, the coupled fluid flow-rock mechanics mass balance equations for Dual Continua become:

$$\frac{\partial\left(\phi^{*i} N_w^i\right)}{\partial t} = -\nabla\cdot\left(v_w^i\right) + q_w^i$$

$$\frac{\partial\left(\phi^{*i} N_o^i\right)}{\partial t} = -\nabla\cdot\left(v_o^i\right) + q_o^i$$

$$\frac{\partial\left(\phi^{*i} N_g^i\right)}{\partial t} = -\nabla\cdot\left(v_g^i + R_o^i v_o^i\right) + q_g^i$$

where

$$q_\alpha^f = q_\alpha + q_\alpha^{m-f}, q_\alpha^m = -q_\alpha^{m-f}$$

$$i = (m, f)$$

$$\phi^{*i} = \left(1-\varepsilon_v\right)\phi^i$$

PRSI Iterative Coupling Approach

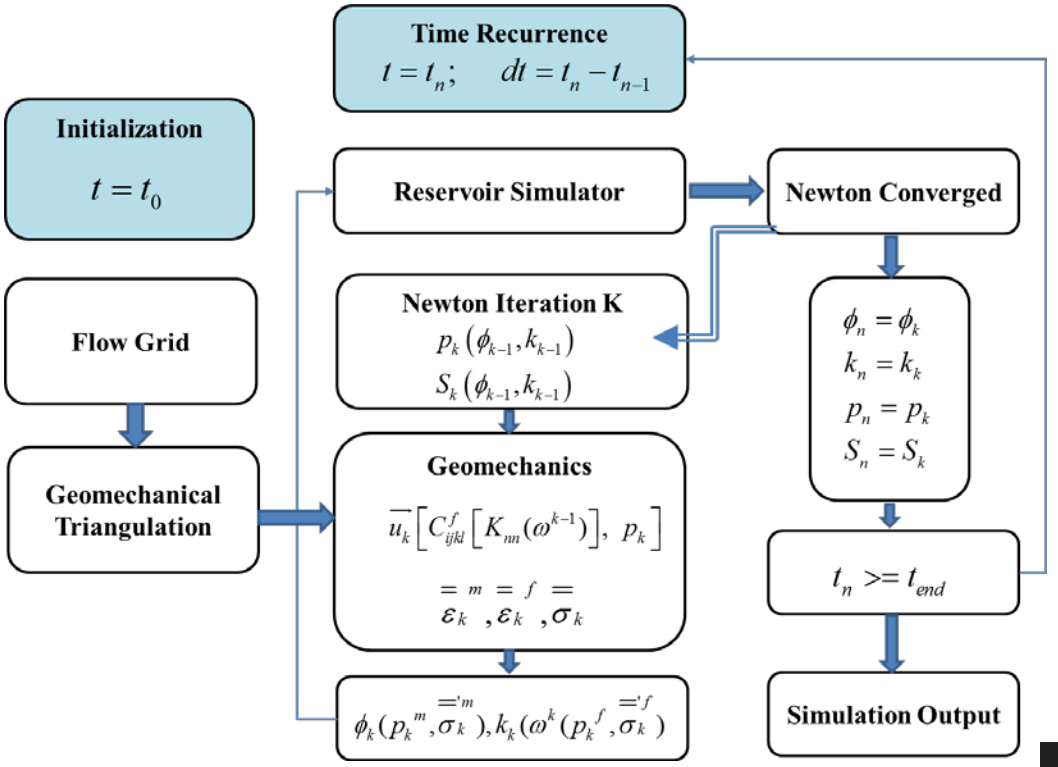

Fracture Deformation Model

Barton-Bandis (1983) Hyperbolic Deformation Model

The Normal Fracture Stiffness:

$$K_n = \frac{\partial \sigma_n}{\partial \Delta\omega} = \frac{1}{a\left(1-\frac{b}{a}\Delta\omega\right)^2} = \frac{K_n^i}{\left(1-\Delta\omega/V^m\right)^2}$$

Fracture Closure:

$$\Delta\omega = \frac{\sigma_n a}{1+\sigma_n a} = \frac{\sigma_n V^m}{K^i{}_n V^m + \sigma_n}$$

Void Fracture Aperture

$$K_{n-hf} = \frac{\partial \delta_n}{\partial \Delta\omega_{hf}} = \frac{K^i_{n-hf}}{\left(1-d\omega^*{}_{hf}/V_{hf}{}^m\right)^2}$$

$$d\omega^*{}_{hf} = f_{hf}\left(\frac{\sigma_n V_{hf}{}^m}{K^i{}_{n\_hf} V_{hf}{}^m + \sigma_n}\right)$$

$$f_{hf} = V_0 \ln\left(1-\frac{d\omega}{V_0}\right)$$

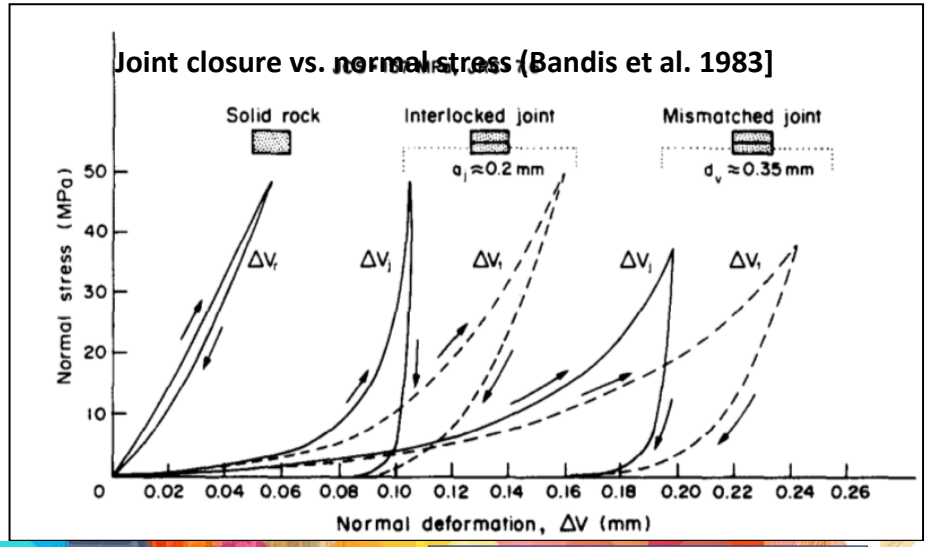

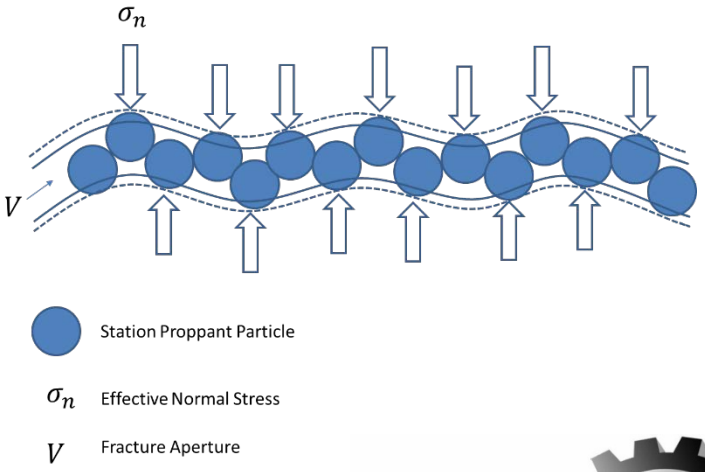

Contact Theory Based Cubic Law

*1: **High-strength Proppant**: Vm=7.62E-4 m; Kni=2E+8 Kpa/m*

*2: **Mid-strength Proppant**: Vm=9.91E-4 m; Kni=2E+7 Kpa/m*

*3: **No Proppant**: Vm=1.14E-4 m; Kni=6E+6 Kpa/m*

UNIVERSITY OF CALGARY

Analytical coupled fracture deformation model

$$k^{'} = k_0^{'}\left(1-\frac{f_{hf}\left(\frac{\sigma_n {V_{hf}}^m}{{K^i}_{n\_hf}{V_{hf}}^m+\sigma_n}\right)}{\omega_0}\right)^3 * \left(\frac{1}{\tau}\right)^n * \left(\frac{1-\bar{a}}{1+\bar{a}}\right)$$

where:

$$\bar{a} = 1-\frac{V}{V_0} \qquad (contact\ area)$$

$$\tau = \frac{V_0}{V} \qquad (fracture-tortuosity)$$

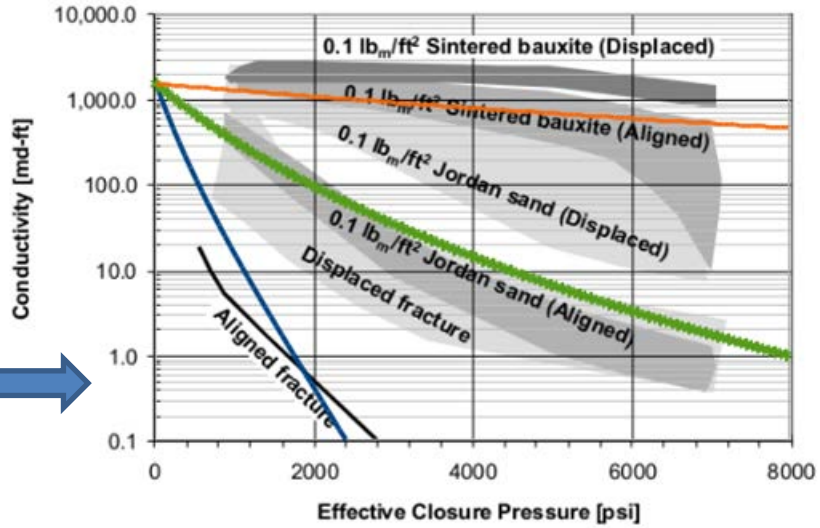

Analytical model validation with experimental results: fracture conductivity vs. effective stress for three types of proppants

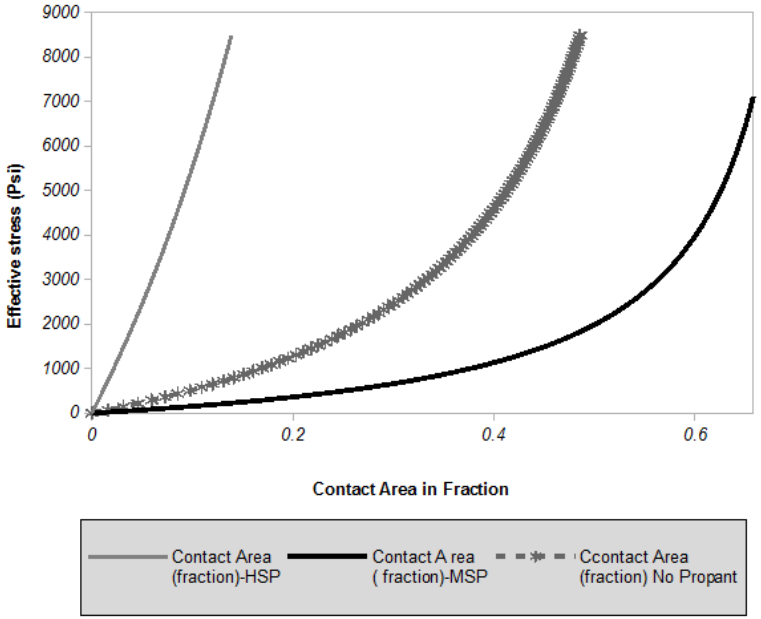

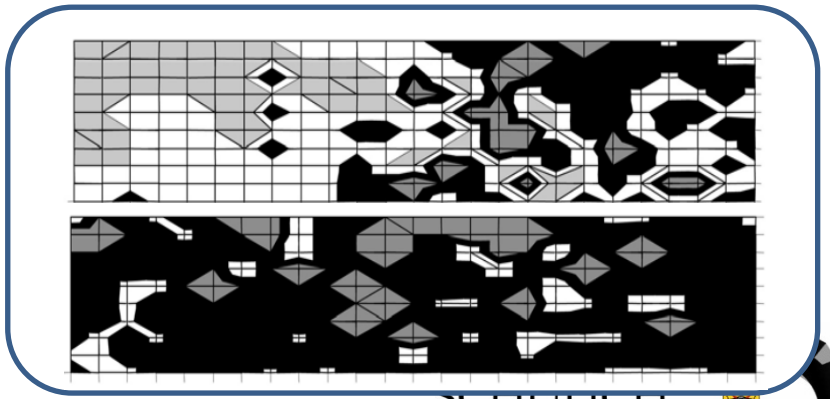

Upper, asperity-crushing correlation profile for Jordan sands; lower, asperity-crushing correlation profile for sintered bauxite (Fred et al., 2001); grey, crushing and low residual fracture width; black, no crushing and high residual fracture width.

Natural Joint Deformation

UNIVERSITY OF CALGARY

Fluid Flow Model

I. Dual-Porosity model based off the quarter symmetry five-spot injection model (Kazemi et al.,1976). The grid in I X J X K is 8 X 8 X 7 with total 448 blocks.

II. The central layer represents the reservoir layer with fracture permeability at 161 mD and matrix permeability at 0.1 mD.

III. The relative permeability to oil and water in fractures covers the full range of saturations from 0 to 1;

IV. The capillary pressure in the fractures declines much faster which induces the imbibition effect of oil-water counter-current flow between the matrix and fractures.

Fracture Deformation Model

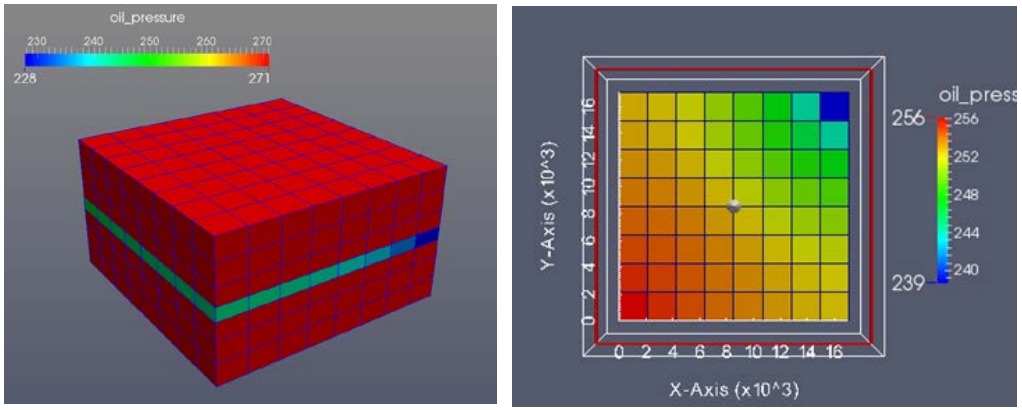

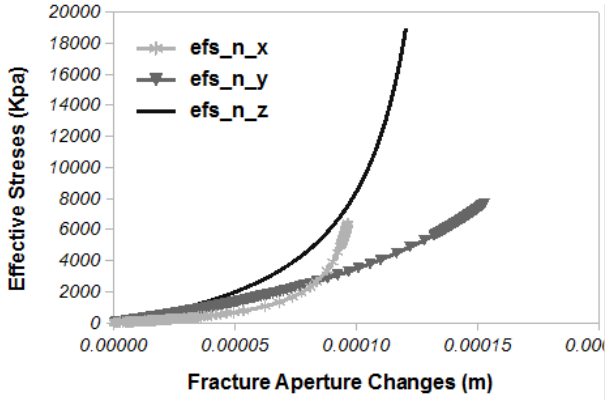

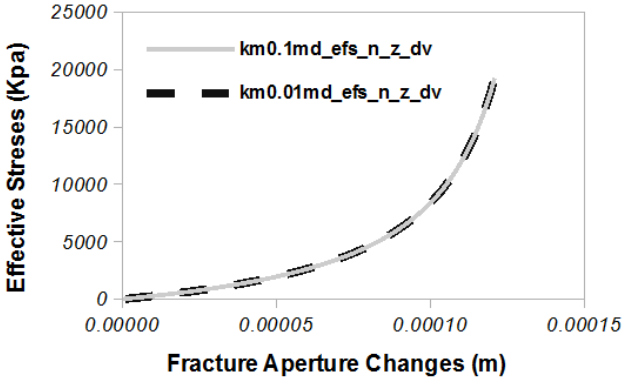

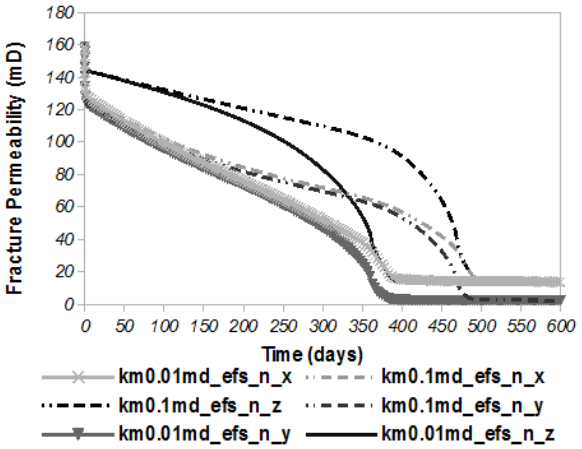

SRV MINC Model

Fluid Flow Model

I. A single stage SRV is setup with 100 ft X 300 ft X 200 ft in geometry and set at TVD 10,500 ft.

II. A dual porosity model is employed with matrix permeability fixed at 0.0005mD and the intrinsic fracture permeability at 150 mD; fracture spacing is set at 10 ft for all three orthogonal directions.

III. Generic PVT data is adopted and modified from Eagle Ford compositional data (Whitson, 2012) and the reservoir is initially under-saturated with initial pressure Pi at 8,000 psi with Pb at 3,500 psi.

IV. Matrix block is discretized into five nested volumes using MINC algorithms

Dual-Porosity vs. MINC

At early time, the dual porosity model underestimates the capillary gradient near the matrix block surface because it assumes the capillary pressure differences between the matrix and fractures over a quasi-steady flow distance of the entire matrix block. Consequently, the MINC method predicts the higher inhibition rates at early time.

At late time, in the MINC method water saturation starts building up near the matrix block surface, which diminishes the capillary pressure gradient driving interporosity flow; therefore, it has a steeper decline in the imbibition rate than the dual porosity approximation, in which all saturation changes are averaged over the entire matrix block.

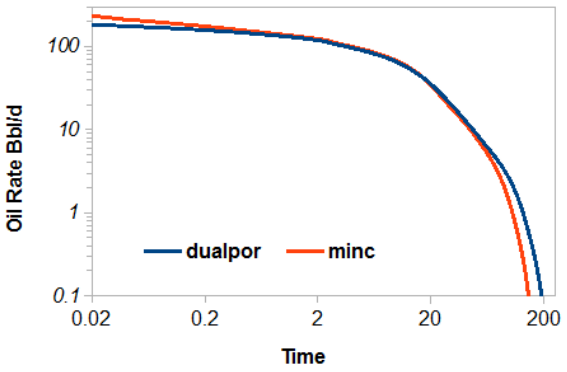

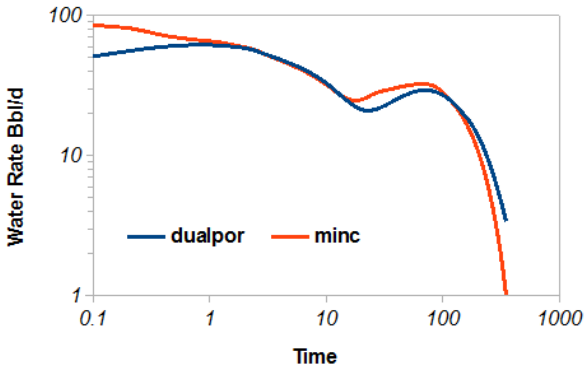

Hybrid Model

Fluid Flow Model

I. The hybrid flow model is set up with 300 ft X 700 ft X 200 ft geometry, which contains the dual porosity SRV with a size of 100 ft X 250 ft X 200 ft.

II. The fracture porosity for the outer tight matrix regions is assigned to zero to mimic the single porosity behavior.

III. The simulation results of the hybrid model show that production has been sustained for a much longer period of time with a very small decline at late time

Element of Symmetry

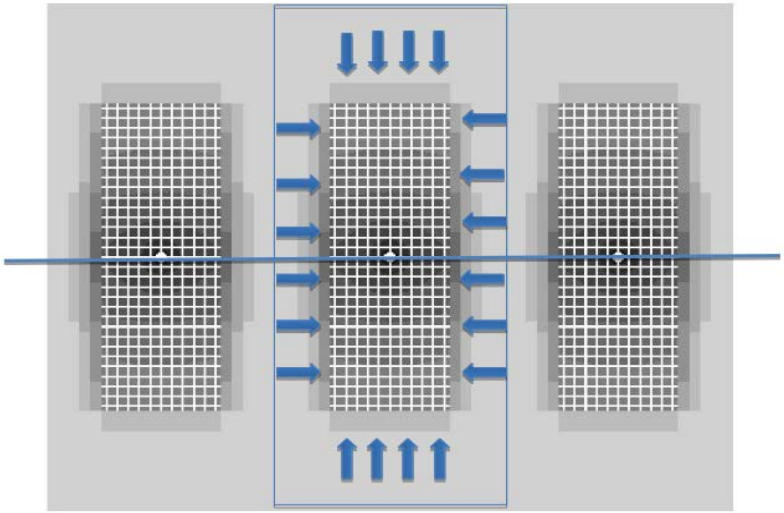

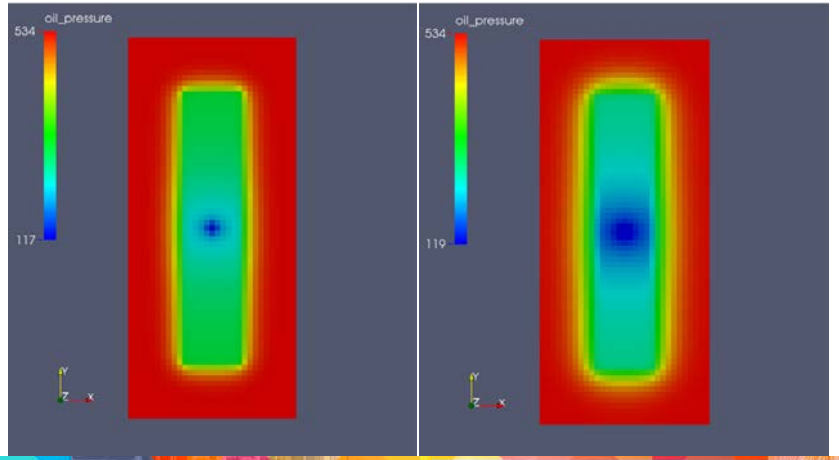

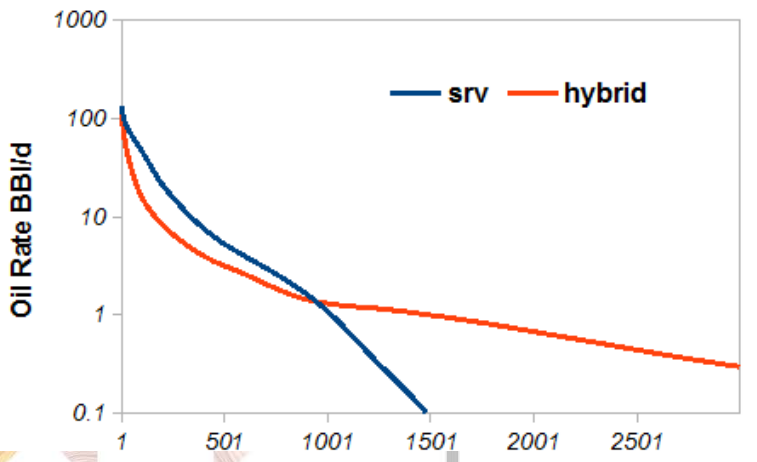

Hydraulic Fracture Deformation Model

UNIVERSITY OF CALGARY

Fracture Deformation Model

I. Three scenarios are built on various fracture permeabilities 1000 mD, 500 mD and 200 mD by assigning the corresponding initial fracture apertures determined by the analytical model.

II. The anisotropic mechanical deformation models are assigned for three orthogonal fracture sets:
   i. Varying the maximum fracture closure Vm and the initial fracture stiffness to represent the high-mid strength proppant filled fracture network;
   ii. Applying an anisotropic stress field to represent the initial in-situ stress conditions;
   iii. A fixed boundary condition in four sides and the bottom plane and only the top plane is allowed to move.

# Frac_Set	V0	Vm	kccf	Strike	Dip	Fracture Spacing	kni
#	(m)	(m)	(md)	(degree)	(degree)	(m)	(kPa/m)
1	2.54E-004	1.27E-004	0.5	0	90	3.048	100000000
2	2.54E-004	1.65E-004	0.5	90	90	3.048	75000000
3	2.54E-004	1.91E-004	0.005	0	0	3.048	50000000

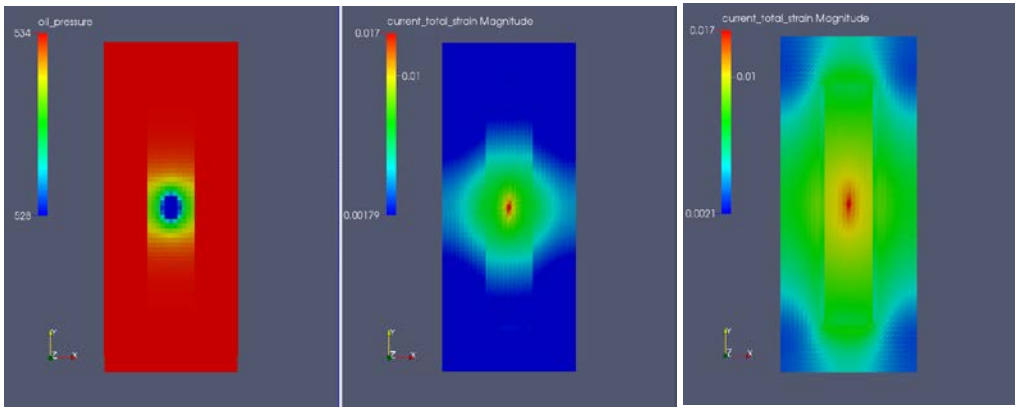

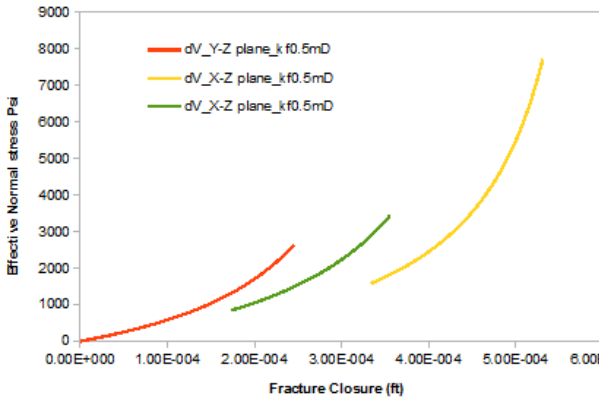

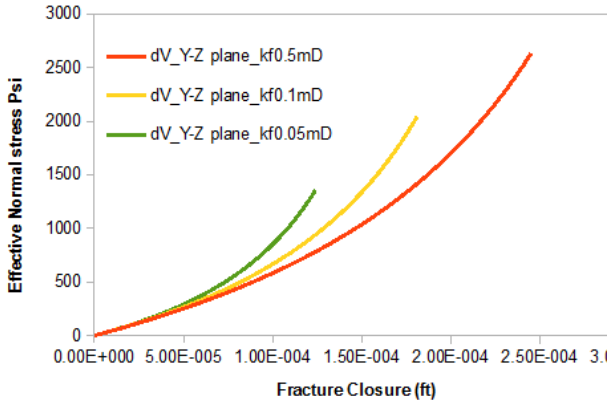

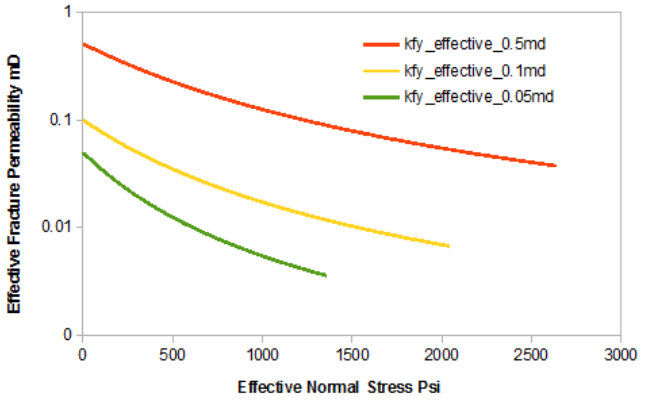

Conclusions I

A coupled flow-stress model provides a dynamic coupling method in predicting the degradation of the fracture conductivity due to proppant crushes and embedment under the loading stress.

I. A dual porosity model for modeling a fractured reservoir has been revisited using a coupled approach. Three orthogonal fractures deform non-uniformly according to each mechanical model assigned. The tighter matrix permeability contributes to the higher pressure drop, which in turn leads to the quicker rising in effective stresses, faster fracture closing, and steeper declining in fracture permeability.

II. Modeling the fluid flow inside a hydraulically fractured network requires a coupled flow-stress simulation platform. The sharp pore pressure declining due to the tight matrix permeability leads to a substantial increase in the effective stress applied on the hydraulic fracture planes. Consequently, fractures start to close under the loading in-situ conditions.

III. A hydraulic fracture deformation model has been developed using a contact theory and validated with published API proppant lab test data. By iterating on the maximum allowable fracture closure and fracture stiffness, the spectra of the hyperbolic deformation functions are generated analytically by fitting the various proppant deformation curves.

Conclusions II

IV. Coupled flow-stress simulations have been carefully designed and implemented using the PRSI framework. A series of numerical experiments have been implemented. Simulation results predict the effective fracture permeability through a wide range of fracture closure and stiffness; in order to achieve the commercial production rate, a certain proppant strength level approximated by the fracture stiffness is required to prevent fractures from closing and maintain conductivity channels for fluid flow.

V. The MINC approach has been adopted in modeling tight oil reservoirs for predicting the transient linear interporosity flow inside matrix blocks and between the matrix and fractures. A conventional simulator tends to underestimate the pressure gradient by averaging over the entire the matrix block domain; the nested meshes method can accurately capture the sharp capillary gradient which drives the interporosity flow between the matrix and fractures.

VI. PRSI has the excellent scalability which has been demonstrated using the full well model with 35 stages hydraulic fractures. 9 times speed up is observed using 144 processors with the total run time at only 30 minutes for the coupled flow-stress model. The parallel speed up has many practical implementations for investigating the well interactions using a sector model and determining the optimal well spacing.